catalysts

MDPI

Article

Effects of Mesopore Internal Surfaces on the Structure of Immobilized Pd-Bisphosphine Complexes Analyzed by Variable-Temperature XAFS and Their Catalytic Performances

Ken Motokura [1,2,*], Takuma Fukuda [1], Yohei Uemura [3], Daiju Matsumura [4], Marika Ikeda [1], Masayuki Nambo [1] and Wang-Jae Chun [5]

1 Department of Chemical Science and Engineering, School of Materials and Chemical Technology, Tokyo Institute of Technology, 4259-G1-14 Nagatsuta-cho, Midori-ku, Yokohama, Kanagawa 226-8502, Japan; fukuda.t.al@m.titech.ac.jp (T.F.); ikeda.m.af@m.titech.ac.jp (M.I.); nambo.m.aa@m.titech.ac.jp (M.N.)
2 Precursory Research for Embryonic Science and Technology (PRESTO), Japan Science and Technology Agency (JST), 4-1-8 Honcho, Kawaguchi 332-0012, Japan
3 Division of Electronic Structure, Department of Materials Molecular Science, Institute for Molecular Science, Myodaiji, Okazaki 444-8585, Japan; y-uemura@ims.ac.jp
4 Materials Sciences Research Center, Japan Atomic Energy Agency, 1-1-1 Sayo-cho Koto, Sayo-gun 679-5148, Japan; daiju@spring8.or.jp
5 Graduate School of Arts and Sciences, International Christian University, Mitaka, Tokyo 181-8585, Japan; wchun@icu.ac.jp
* Correspondence: motokura.k.ab@m.titech.ac.jp; Tel.: +81-45-924-5569

Received: 29 January 2018; Accepted: 5 March 2018; Published: 9 March 2018

Abstract: In this study, mesoporous and nonporous silica-supported Pd complexes were synthesized and characterized. Variable-temperature XAFS measurements and a curve-fitting analysis showed a slightly larger contribution of σ^2_{static} when the Pd complexes were on a nonporous support in comparison to a mesoporous support. In contrast, the catalytic performance of the attached Pd complex in the Suzuki-Miyaura cross-coupling reaction was not affected by such small differences in the static disorder of the Pd complex.

Keywords: mesoporous silica; palladium complex; XAFS; Suzuki-Miyaura coupling reaction

1. Introduction

Mesoporous silica is an ideal support material for the preparation of highly active catalysts because of its high surface area, inert nature of silica, and functionalization ability [1–10]. Among various approaches to functionalizing mesoporous silica, silane-coupling reaction, a reaction between surface silanol and functional molecules containing a trialkoxy group, is one of the most common procedures for the preparation of a supported catalyst. Despite the frequent use of silane-coupling reactions in the functionalization of mesoporous silica materials, it is still a challenge to obtain a detailed analysis of the effect that the internal surface curvature of mesoporous silica has on the structure of the immobilized functionality. This difficulty is mainly due to the generally weak interaction between the silica surface and the immobilized function, as well as their remote location with reference to one another.

X-ray absorption fine structure (XAFS) analysis is a useful technique for determining the detailed local structure of functionalized materials. Recently, we reported a curve-fitting analysis of Pd K-edge extended X-ray absorption fine structure (EXAFS) spectra of SiO_2-supported Pd complexes [11,12]. The study indicated that the Debye-Waller (DW) factors (σ^2) become greater with an increase in the size of the co-immobilized organic molecules. Since the DW factor has contributions from both the

static and dynamic disorders, i.e., $\sigma^2 = \sigma^2_{static} + \sigma^2_{dynamic}$, the variable-temperature XAFS analysis of the supported Pd complex should reveal the contributions of these two functions. For example, static and dynamic disorders are derived from the distorted structure of metal complexes and the thermal vibration of chemical bonds, respectively. Especially at low temperatures (e.g., 20 K), the contribution from thermal disorder becomes negligible, suggesting that the DW value differences of samples is affected by static disorder, the distorted structure of metal complexes. Therefore, variable-temperature XAFS analysis possibly suggests a very small structure change in the Pd complex caused by the structure of the support material.

Herein, we examined the variable-temperature XAFS analysis of both the mesoporous and the nonporous silica-supported Pd-bisphosphine complexes. The study aimed to clarify not only the local structures of the Pd complexes, but also the small differences in their structure. In addition, the catalytic activities of the supported catalysts were evaluated using the Suzuki-Miyaura coupling reaction as a typical Pd-catalyzed reaction.

2. Results and Discussion

Mesoporous silica (MS) samples with different pore diameters were prepared via the sol-gel synthetic method using tetraethoxysilane (TEOS) and primary amines with C8 to C18 carbon chains [13]. The detailed analysis results of synthesized MS were reported previously [12]. The surface areas and average pore diameters of the synthesized MS structures are shown in Table 1. The MS supports using Cn primary amines were denoted as MS(Cn). Nonporous amorphous silica (SiO_2, Aerosil300) was used as a reference material.

Table 1. Physicochemical properties of the silica support.

Support	Surface Area [m^2/g]	Pore Size [Å]
MS(C8)	1865	16
MS(C12)	1175	23
MS(C18)	876	31
SiO_2 [a]	300 ± 30	-

[a] Nonporous SiO_2 (Aerosil300).

The procedure for the preparation of the MS-supported Pd complexes (MS/PP-Pd) is shown in Scheme 1A. The Pd-bisphosphine complex with triethoxysilyl group (PP-Pd) was synthesized by a simple complexation reaction between $[Pd(\eta^3\text{-allyl})Cl]_2$ and a bisphosphine ligand (PP-Pd). The silane coupling reaction of PP-Pd to the respective MS afforded the desired MS/PP-Pd. Solid-state ^{13}C and ^{31}P MAS NMR analysis of the synthesized MS/PP-Pd and SiO_2/PP-Pd complexes indicated the preservation of the carbon chain in the Pd complex and the coordination structure of the Pd bisphosphine complex, respectively [11,12]. Elemental analysis measurements of MS(C12)/PP-Pd indicated 0.26 mmol/g of Pd loading. SEM analysis of the MS-supported samples indicated that the PP-Pd complex was homogeneously dispersed into the mesopores (Figure S1, Supplementary Materials). Additionally, SiO_2, without mesopores, was used as a support material for the PP-Pd immobilization (SiO_2/PP-Pd) (Scheme 1B). The Pd-K edge XAFS analysis of the prepared samples strongly suggested the preservation of the PP-Pd complex structure after immobilization [12].

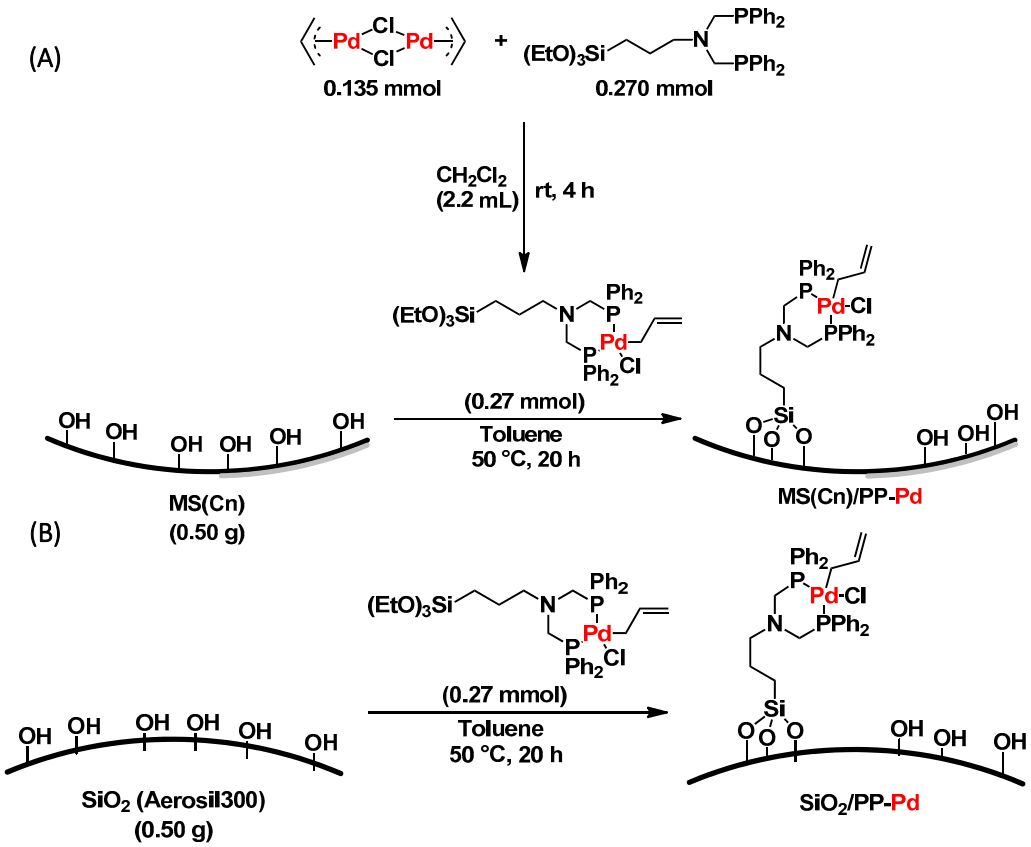

Scheme 1. Synthetic route to catalysts (**A**) MS(Cn)/PP-Pd and (**B**) SiO_2/PP-Pd.

Variable-temperature XAFS measurements were carried out in order to elucidate in detail the effect that the morphology of the silica support has on the PP-Pd complex local structure. Figure 1 presents Pd K-edge X-ray absorption near edge structure (XANES) spectra of MS(C8)/PP-Pd measured from 300 to 20 K, as well as MS/PP-Pd and SiO_2/PP-Pd measured at 20 K. No significant change of the spectra was observed when the temperature was lowered from room temperature to 20 K, which implied that the structure of the Pd complex was preserved during the variable-temperature measurement. The Fourier transforms (FTs) of the k^3-weighted Pd K-edge EXAFS spectra of the samples are summarized in Figure 2. A strong peak at around 1.8 Å that was observed in all the spectra of the samples measured at 20 K was assigned to the Pd-P and Pd-Cl bonds (Figure 2D–G). Table 2 summarizes the results of the curve-fitting analysis of the FT EXAFS spectra of SiO_2/PP-Pd, MS(C18)/PP-Pd, and MS(C8)/PP-Pd at variable temperatures by using Pd-P/Cl parameter. The coordination number (N) was set at 3 due to the two P and one Cl coordination structure of the PP-Pd complex (Scheme 1). The bond distances (r) in all samples were in the range of 2.27 ± 0.01 Å, which is a suitable value for the Pd-P/Cl bonding [14]. The Debye-Waller (DW) factors (σ^2) decreased when the measurement temperature was lowered, indicating that the differences in the contribution of σ^2_{static} to each sample can be evaluated through low temperature measurement ($\sigma^2 = \sigma^2_{static} + \sigma^2_{dynamic}$).

Figure 3 shows plots of the DW factors against the respective measurement temperature for each sample. Considering the mesoporous silica-supported complexes [((□) MS(C8)PP-Pd and ((△) MS(C18)/PP-Pd], the σ^2 value decreased linearly with the decreasing measurement temperature (dotted line). In contrast, for ((○) SiO_2/PP-Pd, the σ^2 value first decreased from 300 to 200 K, and then became almost constant from 200 to 20 K (red solid line). We found a larger DW factor value for SiO_2/PP-Pd compared to MS/PP-Pd in the range from 100 to 20 K. These results indicate that the contribution of $\sigma_{dynamic}$ to SiO_2/PP-Pd is smaller than that to MS/PP-Pd. Also, the highest σ^2 value at 20 K suggests that σ^2_{static} of SiO_2/PP-Pd was larger than that of MS/PP-Pd. In the case

of MS(C12)/PP-Pd, similar trend to MS(C8)PP-Pd and MS(C18)/PP-Pd was observed, as shown in Table S1, Supplementary Materials.

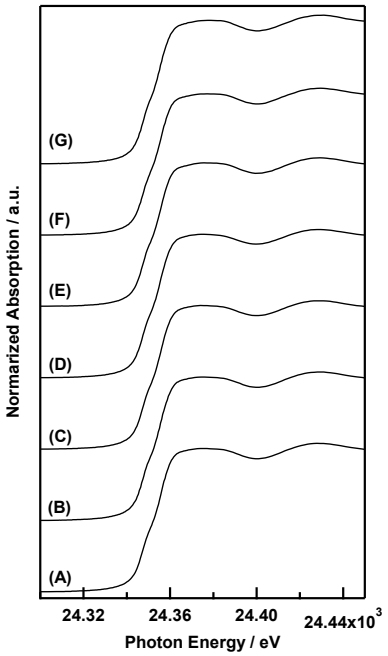

Figure 1. Pd K-edge XANES spectra of MS(C8)/PP-Pd measured at (**A**) 300 K; (**B**) 200 K; (**C**) 100 K; and (**D**) 20 K; (**E**) MS(C12)/PP-Pd measured at 20 K; (**F**) MS(C18)/PP-Pd measured at 20 K; (**G**) SiO_2/PP-Pd measured at 20 K.

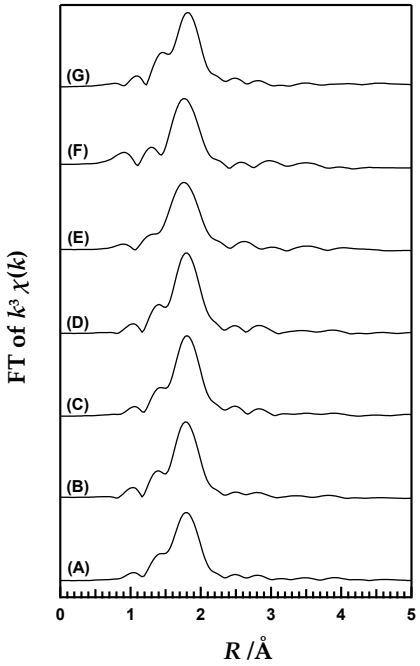

Figure 2. Fourier Transforms of the k^3-weighted Pd K-edge EXAFS spectra of MS(C8)/PP-Pd measured at (**A**) 300 K; (**B**) 200 K; (**C**) 100 K; and (**D**) 20 K; (**E**) MS(C12)/PP-Pd measured at 20 K; (**F**) MS(C18)/PP-Pd measured at 20 K; (**G**) SiO_2/PP-Pd measured at 20 K. The k range for the FT was k = 1.3–13 Å^{-1}.

Table 2. Parameters determined by the curve-fitting analysis of variable-temperature EXAFS spectra of SiO_2/PP-Pd and MS(Cn)/PP-Pd [a].

Temperature [K]	N [b]	r [c] [Å]	σ^2 [d] [Å^2 × 10^{-3}]	ΔE [e] [eV]	Rf [f] [%]
SiO_2/PP-Pd					
300	3	2.27 ± 0.01	3.97 ± 0.05	−10.69 ± 2.05	1.72
200		2.27 ± 0.01	2.64 ± 0.05	−9.94 ± 2.02	3.37
100		2.27 ± 0.01	2.48 ± 0.05	−11.49 ± 2.08	1.90
20		2.28 ± 0.01	2.80 ± 0.05	−9.71 ± 2.09	2.16
MS(C18)/PP-Pd					
300	3	2.27 ± 0.01	3.29 ± 0.05	−11.46 ± 2.05	1.99
200		2.27 ± 0.01	2.64 ± 0.05	−10.79 ± 2.07	1.58
100		2.26 ± 0.01	1.88 ± 0.05	−11.04 ± 2.09	1.91
20		2.27 ± 0.01	1.58 ± 0.05	−10.11 ± 2.09	3.56
MS(C8)/PP-Pd					
300	3	2.27 ± 0.01	3.29 ± 0.05	−11.14 ± 2.05	1.96
200		2.27 ± 0.01	2.33 ± 0.05	−10.85 ± 2.06	2.11
100		2.27 ± 0.01	2.03 ± 0.05	−9.67 ± 2.08	1.53
20		2.27 ± 0.01	1.73 ± 0.05	−11.14 ± 2.09	2.00

[a] Fourier transform and Fourier-filtering regions were limited, where Δk = 2.3~13.0 Å^{-1}. and Δr = 1.0~2.2 Å, respectively. Curve-fitting analysis was performed for the Pd-P/Cl shell. [b] Coordination number was fixed to 3 (two Pd-P and one Pd-Cl bonds). [c] Bond distance between absorber and backscatter atoms. [d] The Debye-Waller factor (DW) accounts for the difference between the sample and reference. [e] The inner potential correction accounts for the difference in the inner potential between the sample and reference. [f] The goodness of curve fit.

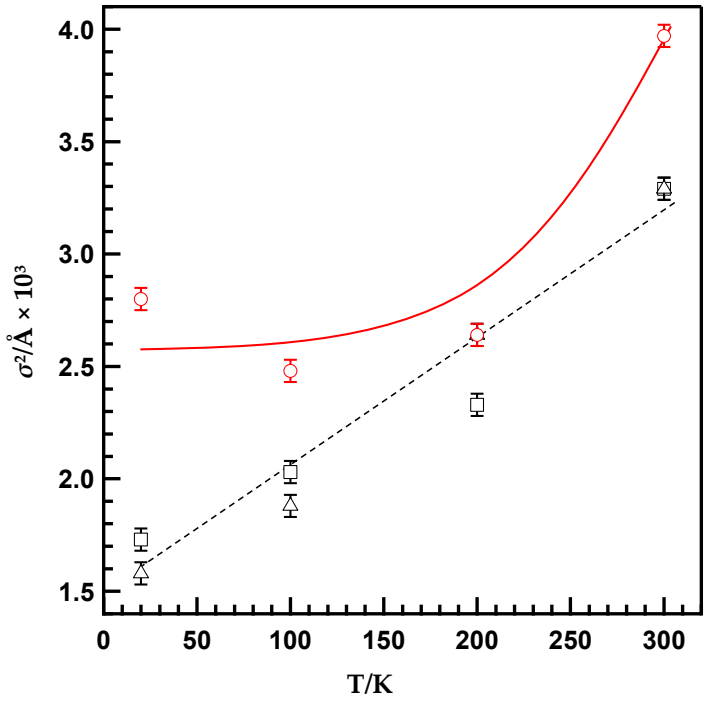

Figure 3. Plots of the DW factors (σ^2) against the measurement temperature for (□) MS(C8)PP-Pd, (△) MS(C18)/PP-Pd, and (○) SiO_2/PP-Pd.

This implies that the Pd complex on a nonporous SiO_2 surface enhanced the static disorder of the local structure of Pd more than the complex on a mesoporous surface. A possible reason for this is the steric stress that was exhibited by the support surface from only one direction (Figure 4A). X-ray reflectivity (XRR) measurements of the metal complex anchored by an alkyl chain to the flat SiO_2 surface indicated the titled structure of a carbon linker, which resulted in the close proximity of the

metal complex and support surface [15]. The relatively homogeneous stress from the mesoporous wall resulted in small σ^2_{static} contribution to MS/PP-Pd (Figure 4B). Interestingly, an effect of the pore size on σ^2static was not observed, suggesting that the effect of pore size on the Pd complex structure is very small in this type of Pd complex.

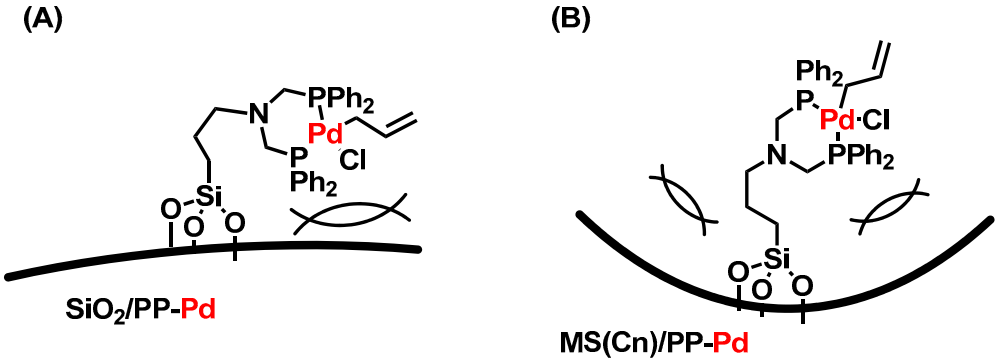

Figure 4. Proposed steric stress mode between the Pd complex and support surface in (**A**) SiO_2/PP-Pd and (**B**) MS(Cn)/PP-Pd.

The effect of the support morphology on the catalytic activity was evaluated using the Suzuki-Miyaura cross-coupling reaction of phenylboronic acid and bromobenzene (Table 3). The results showed that the catalytic activity was not affected by the support structure, and both the nonporous and mesoporous catalysts showed similar product yields (82–90%) and TONs (126–138). This indicates that the differences in the local structure affected by the silica support surface were small, and that they do not influence the catalytic activity of the Pd complex itself. In contrast, the supported catalysts showed much higher product yield than their homogeneous precursor (PP-Pd), which indicates that the Pd complex was stabilized when immobilized on the solid surface.

Table 3. Suzuki-Miyaura coupling reaction of bromobenzene and phenylboronic acid.

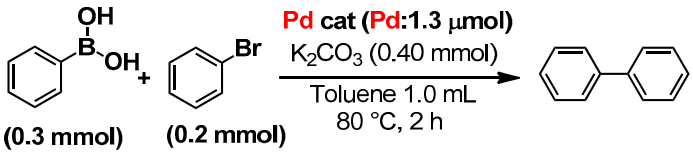

Catalyst	Conv. of Bromobenzene [%]	Yield [%]	TON [Pd^{-1}]
MS(C8)/PP-Pd	91	82	126
MS(C12)/PP-Pd	86	86	132
MS(C18)/PP-Pd	93	90	138
SiO_2/PP-Pd	87	83	128
PP-Pd	82	47	72

Reaction conditions: bromobenznene (0.30 mmol), phenylboronic acid (0.20 mmol), Pd catalyst (Pd: 1.3 μmol), K_2CO_3 (0.40 mmol), toluene (1.0 mL), 80 °C, 2 h.

3. Experimental

3.1. Preparation of Mesoporous Silica (MS)

All the chemicals were purchased from TCI, WAKO, Aldrich, or Kanto Chemical Co. Ltd., Tokyo, Japan. MS(C8, C12, C18) supports with different pore diameters were prepared following a modified version of a previously reported method using primary amines with C8 to C18 alkyl chains as template molecules [13]. An example preparation procedure for MS(C12) is described herein, although a similar procedure was employed for all MS(Cn). Dodecylamine (C12, 53.8 mmol) was dissolved in deionized water (100 g) and ethanol (82 g) at room temperature. Then, tetraethoxysilane (TEOS, 200 mmol) was

added and the solution was vigorously stirred for 30 min at room temperature. The reaction mixture was aged at room temperature for 30 h and the obtained solid was filtered, washed with deionized water, and air-dried. The template amine was removed by mixing with 200 mL of ethanol solution containing 0.1 N HCl for 2 h at 60 °C, and the resulting slurry was filtered. This extraction procedure was performed three times. After that, the obtained solid was mixed with pure ethanol (200 mL) for 2 h at 60 °C, filtered, and dried at 80 °C for 12 h, generating MS(C12).

3.2. Preparation of MS/PP-Pd

All the chemicals were purchased from TCI, WAKO, Aldrich, or Kanto Chemical Co. Ltd., Tokyo, Japan. Treatment of the diphosphine ligand (0.50 mmol) with a solution of $[PdCl(\eta^3\text{-allyl})]_2$ (Pd: 0.50 mmol) in THF (4 mL) for 4 h at room temperature resulted in the desired Pd-bisphosphine complex (PP-Pd) [11]. For detailed characterization of PP-Pd, see ref. [11].

An MS support was pretreated by drying at 120 °C for 3 h under vacuum. The dried MS (0.50 g) was treated with a solution of PP-Pd (0.27 mmol) in toluene (10 mL) at 50 °C for 20 h. After removing the solvent by vacuum evaporation and subsequent drying under vacuum, the desired MS/PP-Pd was generated.

3.3. Variable-Temperature XAFS Measurements

XAFS was measured in transmission mode at Spring-8, BL14B1 (Hyogo, Japan) at 300, 200, 100, 50, and 20 K. The synchrotron radiation from the storage ring was monochromatized with a Si(311) double crystal monochrometer. Ionization chambers filled with Ar gas were used as detectors for monitoring incident (I_0) and transmitted X-rays (I). The angle of the monochromator was calibrated using Pd foil, with the inflection point at the edge set to 24352.6 eV.

XAFS spectra were analyzed using REX2000 (for curve-fitting analysis, Rigaku. Co., Tokyo, Japan). The backscattering amplitude and phase shift of Pd-P/Cl were extracted from the $PdCl_2(PPh_3)_2$ complex.

A goodness of curve fit was estimated using the following equation.

$$R_{factor} = \sqrt{\frac{k^n\chi_{exp}(k) - k^n\chi_{cf}(k)}{k^n\chi_{exp}(k)}}$$

where $\chi_{exp}(k), \chi_{cf}(k)$ are the experimental data and theoretical curve-fitted data, respectively.

3.4. Suzuki-Miyaura Cross Coupling Reaction

All the chemicals were purchased from TCI, WAKO, Aldrich, or Kanto Chemical Co. Ltd., Tokyo, Japan. The prepared MS-supported Pd catalyst (1.3 μmol), toluene (1.0 mL), K_2CO_3 (0.40 mmol), bromobenzene (0.30 mmol), and phenylboronic acid (0.20 mmol) were placed in a Pyrex glass reactor (Tokyo Kasei, Tokyo, Japan). The resulting mixture was stirred vigorously for 2 h at 80 °C under Ar. The formation of biphenyl was confirmed by GC-MS (QP202SE, Shimadzu, Kyoto, Japan). The yield and conversion were determined by GC analysis of a reaction mixture using the internal standard technique.

4. Conclusions

The effect of the support morphology on the attached Pd complex was evaluated by variable-temperature XAFS analysis. The nonporous SiO_2 support showed a relatively larger contribution of σ^2_{static} than the mesoporous support. This result suggests that the Pd complex has a slightly disordered structure due to the steric stress applied by the support surface. However, this small difference in the Pd complex structure did not affect its catalytic activity in the Suzuki-Miyaura cross-coupling reaction. This study proved that variable-temperature XAFS analysis could successfully elucidate long-range interactions between a metal complex and its support surface.

Supplementary Materials: The following are available online at http://www.mdpi.com/2073-4344/8/3/106/s1, Figure S1: SEM image of MS(C8)/PP-Pd and line analysis results for Si, P, and Pd elements, and Table S1: Parameters determined by the curve-fitting analysis of variable-temperature EXAFS spectra of MS(C12)/PP-Pd.

Acknowledgments: XAFS measurements were conducted under the approval of the SPring-8 and the Photon Factory Advisory Committee (2016G025). This study was supported by the JSPS Grant-in-Aid for Scientific Research on Innovative Areas (Grant nos. 16H01010 and 26105003) and Cooperative Research Program of the Institute for Catalysis, Hokkaido University (Grant #17A1002).

Author Contributions: K.M. conceived the project. T.F., Y.U., D.M., and M.I. performed the experiments and spectral analysis. M.N. and W.-J.C. discussed the experiments and results.

Conflicts of Interest: There are no conflicts of interest to declare.

References

1. Cheng, T.; Zhao, Q.; Zhang, D.; Liu, G. Transition-metal-functionalized ordered mesoporous silicas: An overview of sustainable chiral catalysts for enantioselective transformations. *Green Chem.* **2015**, *17*, 2100–2122. [CrossRef]
2. Opanasenko, M.; Štěpnička, P.; Čejika, J. Heterogeneous Pd catalysts supported on silica matrices. *RSC Adv.* **2014**, *4*, 65137–65162. [CrossRef]
3. Rostamnia, S.; Doustkhah, E. Nanoporous silica-supported organocatalyst: A heterogeneous and green hybrid catalyst for organic transformations. *RSC Adv.* **2014**, *4*, 28238–28248. [CrossRef]
4. Conley, M.P.; Copéret, C.; Thieuleux, C. Mesostructured hybrid organic-silica materials: Ideal supports for well-defined heterogeneous organometallic catalysts. *ACS Catal.* **2014**, *4*, 1458–1469. [CrossRef]
5. Yu, C.; He, J. Synergic catalytic effects in confined spaces. *Chem. Commun.* **2012**, *48*, 4933–4940. [CrossRef] [PubMed]
6. Yokoi, T.; Kubota, Y.; Tatsumi, T. Amino-functionalized mesoporous silica as base catalyst and adsorbent. *Appl. Catal. A Gen.* **2012**, *421–422*, 14–37. [CrossRef]
7. Linares, N.; Serrano, E.; Rico, M.; Balu, A.M.; Losada, E.; Luque, R.; García-Martínez, J. Incorporation of chemical functionalities in the framework of mesoporous silica. *Chem. Commun.* **2011**, *47*, 9024–9035. [CrossRef] [PubMed]
8. Lee, I.; Albiter, M.A.; Zhang, Q.; Ge, J.; Yin, Y.; Zaera, F. New nanostructured heterogeneous catalysts with increased selectivity and stability. *Phys. Chem. Chem. Phys.* **2011**, *13*, 2449–2456. [CrossRef] [PubMed]
9. Brühwiler, D. Postsynthetic functionalization of mesoporous silica. *Nanoscale* **2010**, *2*, 887–892. [CrossRef] [PubMed]
10. Slowing, I.I.; Vivero-Escoto, J.L.; Trewyn, B.G.; Lin, V.S.-Y. Mesoporous silica nanoparticles: Structural design and applications. *J. Mater. Chem.* **2010**, *20*, 7924–7937. [CrossRef]
11. Motokura, K.; Saitoh, K.; Noda, H.; Chun, W.-J.; Miyaji, A.; Yamaguchi, S.; Baba, T. A Pd-bisphosphine complex and organic functionalities immobilized on the same SiO_2 surface: Detailed characterization and its use as an efficient catalyst for allylation. *Catal. Sci. Technol.* **2016**, *6*, 5380–5388. [CrossRef]
12. Motokura, K.; Ikeda, M.; Nambo, M.; Chun, W.-J.; Nakajima, K.; Tanaka, S. Concerted catalysis in tight spaces: Palladium-catalyzed allylation reactions accelerated by accumulated active sites in mesoporous silica. *ChemCatChem* **2017**, *9*, 2924–2929. [CrossRef]
13. Tanev, P.T.; Pinnavaia, T.J. A neutral templating route to mesoporous molecular sieves. *Science* **1995**, *267*, 865–867. [CrossRef] [PubMed]
14. Corrêa, R.S.; Graminha, A.E.; Ellena, J.; Batista, A.A. Weak C–H···Cl–Pd interactions toward conformational polymorphism in *trans*-dichloridobis(triphenylphosphane)palladium(II). *Acta Cryst.* **2011**, *C67*, m304–m306.
15. Noda, H.; Motokura, K.; Wakabayashi, Y.; Sasaki, K.; Tajiri, H.; Miyaji, A.; Yamaguchi, S.; Baba, T. Direct estimation of the surface location of immobilized functional groups for concerted catalysis using a probe molecule. *Chem. Eur. J.* **2016**, *22*, 5113–5117. [CrossRef] [PubMed]